Cluster-Assembled Materials: Toward Nanomaterials with Precise Control over Properties

Meichun Qian,[†] Arthur C. Reber,[†] Angel Ugrinov,[‡] Nirmalya K. Chaki,[‡] Sukhendu Mandal,[‡] Héctor M. Saavedra,[‡] Shiv N. Khanna,[†,*] Ayusman Sen,[‡,*] and Paul S. Weiss[‡,§,⊥,*]

[†]Department of Physics, Virginia Commonwealth University, Richmond, Virginia 23284, [‡]Department of Chemistry, The Pennsylvania State University, University Park, Pennsylvania 16802, [§]Department of Physics, The Pennsylvania State University, University Park, Pennsylvania 16802, and [⊥]California NanoSystems Institute and Department of Chemistry and Biochemistry, University of California, Los Angeles, Los Angeles, California 90095

ABSTRACT One pathway toward nanomaterials with controllable band gaps is to assemble solids where atomic clusters serve as building blocks, since the electronic structures of clusters vary with size and composition. To study the role of organization in cluster assemblies, we synthesized multiple architectures incorporating As_7^{3-} clusters through control of the countercations. Optical measurements revealed that the band gaps vary from 1.1—2.1 eV, even though the assemblies are constructed from the identical cluster building block. Theoretical studies explain this variation as being a result of altering the lowest unoccupied molecular orbital levels by changing the countercations. Additional variations in the gap are made by covalently linking the clusters with species of varying electronegativity to alter the degree of charge transfer. These findings offer a general protocol for syntheses of nanoassemblies with tunable electronic properties.

KEYWORDS: cluster-assembled materials · Zintl-ions · band-gap · diffuse reflectance spectroscopy · nanomaterials

Cluster-assembled materials are of interest because they exploit the uniqueness of clusters and situate them among potentially functional materials.[1−17] These materials serve as a link between the predictable size-invariant properties of solids and the evolution in properties observed at the subnanometer scale where every atom counts.[4−10,18−22] Indeed, chemical, electronic, and magnetic properties of clusters are found to vary markedly with size and composition due to both quantum confinement and chemical interactions. Recent synthetic advances confirm that the constructed materials can retain the characteristics of the original building blocks.[14−16] The fundamental question is, what controls the properties of the material once the clusters are incorporated? The important role of countercations in determining the electronic structure of cluster-assembled materials has been discussed previously,[23,24] however a direct correlation between the theoretical calculations based on actual crystal structures and experimentally measured band gaps has not been reported. Here, we show that the electronic properties of cluster-assembled materials derived from anionic Zintl clusters are controlled by the nature of the countercations and the degree of charge transfer to the cluster.

Among the various classes of cluster-assembled materials,[4−11,22,25] Zintl clusters allow a comprehensive study of the effects of architectures with different dimensionality on physical properties.[26−29] Zintl phases form crystalline solids from the combination of heavy post-transition metals with electropositive elements such as the alkali metals. We identified As_7^{3-} as one of the potential building blocks for such a demonstration.[14] The As_7 cluster typically requires three additional electrons to complete its electronic shell. When combined with alkali metals, charge transfer from the alkali atoms to the As cluster results in a As_7^{3-} anion that is surrounded by alkali metal cations, thereby forming compact and crystalline cluster assemblies.[28] While such cluster solids have been known for some time,[26−29] they serve as an ideal test for probing the materials properties and determining the parameters that control them in a variety of cluster assemblies.[4−10] Our results further underscore the ability to tune the properties of cluster-assembled materials by judicious selection of alkali metal countercations or covalent transition metal linkers.

RESULT AND DISCUSSION

We undertook the synthesis and characterization of a wide variety of As_7^{3-}-based cluster assemblies with different countercations, and measured their optical band

*Address correspondence to snkhanna@vcu.edu, asen@chem.psu.edu, psw@cnsi.ucla.edu.

Received for review August 17, 2009 and accepted December 10, 2009.

Published online December 28, 2009. 10.1021/nn9010297

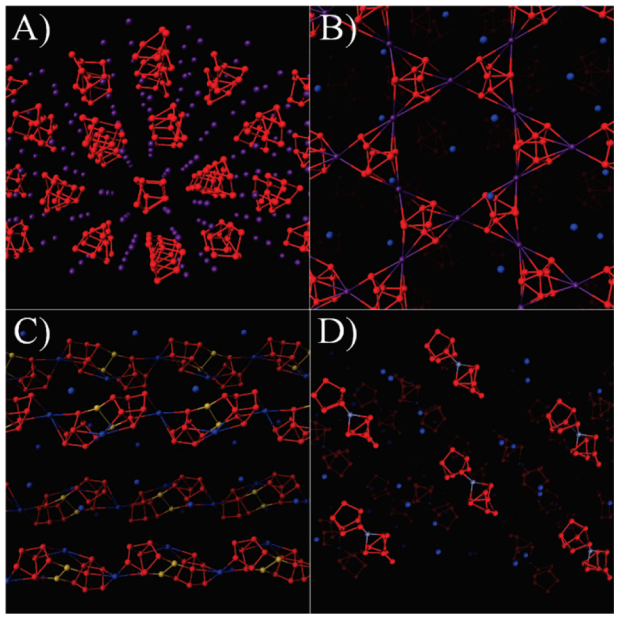

Figure 1. X-ray crystallographic structures of (A) three-dimensional material of As_7Cs_3 (compound 1); (B) two-dimensional sheet of As_7 clusters bound by Cs^+ (compound 3), with $(K\text{-Crypt})^+$ separating these layers; (C) one-dimensional arrangement of $Au_2(As_7)_2^{4-}$ clusters linked by naked K^+ and separated by additional $(K\text{-Crypt})^+$ (compound 7); (D) zero-dimensional $Zn(As_7)_2(K\text{-Crypt})_4$ clusters in the solid state (compound 5). Arsenic atoms are shown in red, cesium in purple, potassium in blue, zinc in gray, and gold in gold. In panel A, the interactions of Cs^+ with As_7 for compound 1 are not shown, while $(K\text{-Crypt})^+$ are indicated only as isolated K^+ in panels B–D for clarity.

gaps to determine how the electronic properties were affected. These clusters were crystallized in the presence of the polycyclic multidentate ligand, 4,7,13,16,21,24-hexaoxa-1,10-diazabicyclo[8.8.8]hexacosane (commonly known as cryptand-222; henceforth "Crypt"), and structurally characterized using X-ray crystallography (Figure 1 and Figure S2; Tables S1a and S1b). All of these cluster assemblies are synthesized either directly (compound **1**) or from the reaction of As_7A_3 [A = K, Rb, Cs] in ethylenediamine with K or Cs (compound **2**–**4**).[30] The precursor, As_7A_3, was directly synthesized in bulk from the corresponding elements in ethylenediamine. We also synthesized the complementary As_{11}^{3-}-based assemblies but here focus on As_7^{3-}-based assemblies.

The selection of Crypt as a cation sequestering agent facilitates the syntheses of Cs-linked cluster assemblies due to Crypt's selective sequestering ability for K^+ and Rb^+ over Cs^+ (Figure S1A). Figure S1B shows the accessible triangular and tetragonal faces of the As_7 cluster, which can be utilized for chemical modifications and for constructing assemblies with direct ionic linkages in one, two, or three dimensions. Similar As_7-based assemblies were synthesized in our laboratory to delineate the effect of alkali metal linking on the optical band gaps (Figure 1). For example, Figure 1A shows the As_7Cs_3 (compound **1**), where the As_7 motifs are linked through Cs^+ in all three dimensions, while $As_7Cs_{1.5}(K\text{-Crypt})_{1.5}$ (compound **3**), shown in Figure 1B, consists of two-dimensional sheets of As_7 clusters separated by cryptated K cations. Several other cluster assemblies linked by alkali metals ions, as described in Table 1, are provided in a supplemental figure (Figure S2).

TABLE 1. Experimentally Measured and Theoretically Calculated Band Gaps for the As_7-Based Cluster-Assembled Materials

compound	cluster formula	band-gap (eV) experimental	band-gap (eV) theoretical
	Building Unit: As_7^{3-}		
1	As_7Cs_3	1.09 ± 0.052	1.19
2	$As_7Cs_2(K\text{-Crypt})$	2.04 ± 0.12	1.98
3	$As_7Cs_{1.5}(K\text{-Crypt})_{1.5}$	2.08 ± 0.05	1.84
4	$As_7Cs_{1.5}(Rb\text{-Crypt})_{1.5}$	1.77 ± 0.021	1.80
	Building Unit: $T(As_7)_2^{4-}$ (T = Zn and Au)		
5	$Zn(As_7)_2(K\text{-Crypt})_4$	1.99 ± 0.052	1.97
6	$Au_2(As_7)_2(K\text{-Crypt})_4$	1.69 ± 0.016	1.68
7	$Au_2(As_7)_2K_2(K\text{-Crypt})_2$	1.46 ± 0.021	1.43

The variations in the architectures and compositions of the assemblies lead to different electronic, optical, and other properties. To demonstrate this, we measured the optical band gaps of cluster-assembled materials using diffuse reflectance spectroscopy, and the Kubelka–Munk model.[31–33] This two-flux model, which considers only diffuse light, is used to determine the absorption coefficients from a surface that both scatters and absorbs incident radiation. For a crystalline solid with a band gap (E_{bg}), the frequency dependence (ν) of the absorption coefficient (κ) can be approximated as

$$\kappa(\nu) = \frac{B_T(h\nu - E_{bg})^n}{h\nu},$$

where B_T is a constant derived from the square of the averaged dipolar momentum matrix element, and n is equal to 0.5 and 2 for *direct* and *indirect* band gap transitions, respectively.[34–37] Using the above equation, the band gap of a material can be obtained by extrapolating to zero with the linear fit to a plot of $(\kappa h\nu)^{1/n}$ *versus* $h\nu$. Figures 2 and S3 show the Tauc plots for the measured cluster assemblies; the corresponding determined values of the band gaps are listed in Table 1. The linearity and agreement with the Tauc relation for both $n = 0.5$ (Figure S3) and $n = 2$ (Figure 2) indicate the presence of both direct and indirect optical transitions, respectively. However, all the compounds have indirect transitions (Figure 2) with band gaps smaller than the direct ones (Figure S3).

We observe significant variations in the band gaps of different cluster-assembled materials made from the same As_7 cluster building block. For example, As_7Cs_3 (compound **1**) has $E_{bg} = 1.09$ eV, while $As_7Cs_2(K\text{-Crypt})$ (compound **2**) has $E_{bg} = 2.04$ eV. The experimental results also reveal general trends regarding the band gaps in these cluster-assembled materials. For example, the

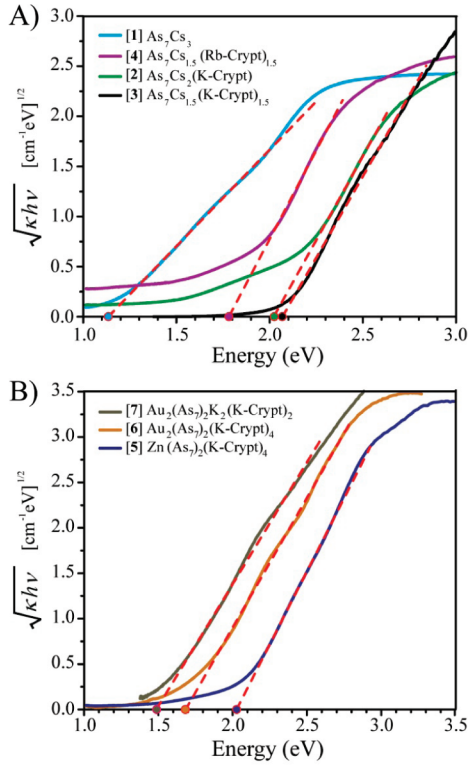

Figure 2. Tauc plots showing the band gaps determined from the optical absorption spectra (see text) of (A) alkali−metal-linked As_7 cluster assemblies (compounds 1−4) and (B) cluster assemblies with either Zn or Au covalently bound to As_7 (compounds 5−7).

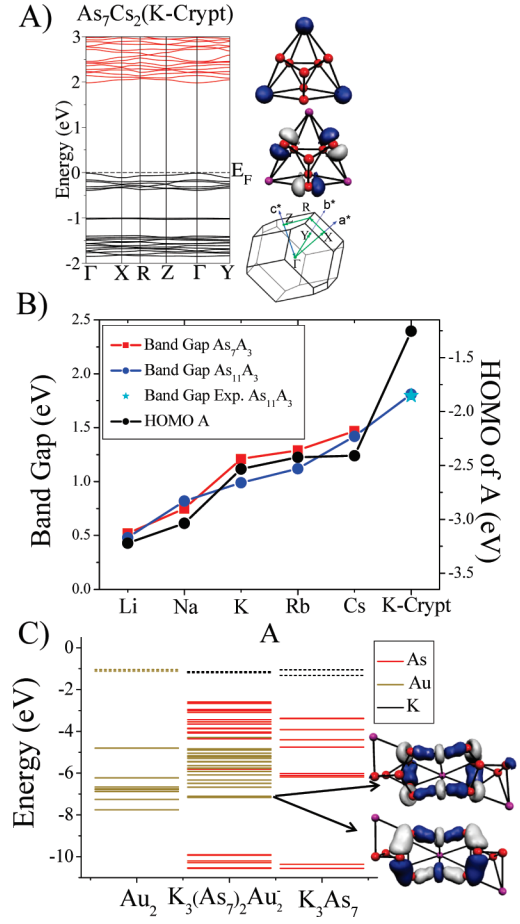

Figure 3. (A) Band plots of As_7Cs_2(K-Crypt) with the frontier orbitals of the clusters shown. (B) Band gaps of As_7A_3 and $As_{11}A_3$ Zintl phases and the HOMOs of the neutral atoms. (C) A molecular orbital diagram of Au_2, $K_3(As_7)_2Au_2^-$ and K_3As_7 and the charge densities of the covalent bonds between the gold atoms and the arsenic clusters (A = alkali metal).

two-dimensional sheets, $As_7Cs_{1.5}$(K-Crypt)$_{1.5}$ (compound **3**) and As_7Cs_2(K-Crypt) (compound **2**), have larger band gaps, E_{bg} = 2.08 and 2.04 eV, respectively, while the three-dimensional assembly, As_7Cs_3 (compound **1**), has a lower band gap, E_{bg} = 1.09 eV. Cluster assemblies made from the same motif should be isoelectronic, yet the band gap is almost doubled on moving from Cs to cryptated K.

To delineate the roles of various atoms and clusters, first principles electronic structure investigations were undertaken to probe the electronic band structure and the nature of the electronic states marking the set of highest occupied and lowest unoccupied molecular orbitals (HOMO and LUMO, respectively). All the calculations were carried out within a gradient corrected density functional formalism with two complementary schemes. The calculations on periodic solids were carried out using a plane-wave basis set with the projector augmented plane-wave method, while some representative clusters were studied using a real space linear combination of atomic orbitals molecular orbital approach, to investigate local effects. The calculations on the bulk solids have been performed on the basis of X-ray crystallographic structures (Figure 1 and Figure S2), and the details are provided in the methods and Supporting Information.[30]

Figure 3A shows the band structure of the As_7Cs_2(K-Crypt) solid. The energy bands have very low dispersion, attributed to the fact that As_7^{3-} motifs are separated from each other by the alkali cation and do not interact directly. The As_7^{3-} motif is a closed-shell species stabilized by charge transfer from alkali atoms, the latter thereby also acquiring closed-shell configurations. Consequently, the resulting solid is a semiconductor (as the valence band is completely full and separated from the conduction band). The energy bands have low dispersion, which should result in large effective masses of the carriers. On the other hand, the weak intercluster interactions may lead to soft phonon modes. Combinations of these features could be expected to lead to novel transport properties, such as the high superconducting transition temperatures in alkali-linked fullerides.[38] A key property is the band gap, and Table 1 shows the theoretical values obtained from the band structure calculations of the solids of compounds **1**−**4**. The calculated band gaps are in good agreement with the corresponding experimentally measured band gaps. Note that the density functional calculations are known to underestimate the band gap in bulk semiconductors.[39] In cluster solids, the band

gaps are associated with weakly broadened localized states in cluster motifs, which are better described by density functional theory.

The cluster solid is essentially an assembly of As_7A_3 motifs and hence its electronic spectrum can be regarded as electronic states of As_7A_3 motifs modified by the architecture of the assembled unit. The electronic states in the individual components are only mildly broadened by the collective assembly, and the clusters' varying local environment causes small shifts in the bands. To probe the origins of the varying band gaps, we therefore examined the nature of their frontier orbitals in isolated As_7A_3 clusters. We analyzed the electronic states marking the HOMOs and the LUMOs and plotted the charge densities of As_7A_3 (shown in Figure 3A). While the HOMO is composed almost entirely of contributions from the As atoms, the LUMO is mainly localized on the alkali metal cations. This indicates that the orbital on the countercation and not the electronic structure of the As cluster building block primarily controls the position of the LUMO. The LUMO of the material is therefore derived from the absolute position of the HOMO of the neutral alkali metal atom. This close correlation is seen in Figure 3B, which shows the energies of the HOMOs of the alkali metal atoms and the calculated band gaps of the pure Zintl materials. These were obtained by calculating the band structures of optimized As_7A_3 and $As_{11}A_3$ assemblies for various alkali atoms in the observed orthorhombic and monoclinic structures of As_7Cs_3 and $As_{11}Cs_3$.[28,29] The experimental and theoretical band gaps for $As_{11}(K\text{-}Crypt)_3$ are also included, because $As_7(K\text{-}Crypt)_3$ cannot be crystallized. The HOMO of the free neutral atom is lowest for lithium and increases as the size of the atom increases, except for the cryptated potassium, in which the lone pair on the polyether greatly destabilizes the HOMO. There is mixing of the states in solids with mixed countercations, as replacing a single Cs atom with cryptated K ions results in an increase of E_{bg} from 1.1 to 2.1 eV; so, the composition of the countercation is the dominant feature, which controls the band gap in these alkali metal linked Zintl clusters-assemblies. Our calculations suggest the effective upper limit of the band gap of these cluster materials to be *ca.* 2.5 eV, which is the effective HOMO−LUMO gap of As_7^{3-}.

While the variation of the LUMO seems to dominate in solids, our studies in finite clusters indicate that the band gap is also dependent on the degree of charge transfer. To probe the effect of charge transfer, we investigated the effect on the band gap of covalent linkers with varying electronegativity. These assemblies are synthesized from the reaction of As_7K_3 in ethylenediamine with $Zn(C_6H_5)_2$ (compound **5**), and $AuP(C_6H_5)_3Cl$ (compounds **6**−**7**).[30] The crystal structures of $Zn(As_7)_2(K\text{-}Crypt)_4$ (compound **5**) and $Au_2(As_7)_2(K\text{-}Crypt)_4$ (compound **6**) revealed that two As_7 units are linked by one Zu and two Au atoms, respectively, while $(K\text{-}Crypt)^+$ ions balance the additional charges. The $Au_2(As_7)_2^{4-}$ building unit can further be arranged in a one-dimensional fashion as $Au_2(As_7)_2K_2(K\text{-}Crypt)_2$ (compound **7**) by controlling the ratio of naked and cryptated K^+. The one- and zero-dimensional arrangements of $Au_2(As_7)_2^{4-}$ and $Zn(As_7)_2^{4-}$ are shown in Figure 1 panels C and D, respectively. Band gaps of these three cluster-assemblies (compound **5**−**7**) have been measured experimentally and compared with the theoretical values (Table 1).

The formation of this stable crystal, $Au_2(As_7)_2K_2(K\text{-}Crypt)_2$, was quite interesting since the ionization potential of a Au atom is 9.22 eV, compared to 4.34 eV for K. The substitution of K by Au is not expected to result in the same donation of charge. First principles electronic structure calculations on a representative $(As_7)_2Au_2K_3^-$ cluster were carried out using effective core potentials that include relativistic effects to represent the Au atoms. Figure 3C shows the one-electron levels in an isolated Au_2 molecule, an $(As_7)_2Au_2K_3^-$ cluster, and an isolated As_7K_3 cluster. The electron levels that have appreciable contributions from Au sites are shown in gold. The Au atoms form deep bonding states in the $(As_7)_2Au_2K_3^-$ clusters, indicative of covalent interactions. This is further confirmed by the charge density in the Au-rich orbitals shown in Figure 3C. The covalent bond between the Au and arsenic cluster's lone pair also reduces the number of K atoms required to stabilize the resulting solid from three to two.

We theoretically investigated the electronic structures of these covalently linked cluster assemblies to understand the band gap variations, encouraged by the excellent agreement between calculated and experimentally measured band gaps. First, we replaced the two K atoms in $Au_2(As_7)_2K_2(K\text{-}Crypt)_2$ by two $(K\text{-}Crypt)^+$ to form $Au_2(As_7)_2(K\text{-}Crypt)_4$, which resulted in an increase of the band gap due to countercation effects, as previously noted. Further, Au atoms are monovalent and one could stabilize the solid by replacing two Au atoms by a single divalent atom such as Zn. Indeed, the structure of $Zn(As_7)_2(K\text{-}Crypt)_4$ was similar to that of $Au_2(As_7)_2(K\text{-}Crypt)_4$ except that Au_2 is replaced by a single Zn atom. While the structure is similar, the substitution of Au_2 by Zn increases the band gap from 1.69 to 1.99 eV (Table 1). To probe the origins of this increase, representative electronic structure studies on $(As_7)_2ZnK_4$ were carried out and the results compared with those for $(As_7)_2Au_2K_4$ clusters. A Hirshfeld charge analysis indicated that while the net charge on each Au atom is −0.02, the charge on the Zn sites is +0.17, showing greater charge transfer to the arsenic motif in the Zn assembly. As the enhanced charge transfer lowers the HOMO states on the arsenic anion, a decrease in the electronegativity of the linker results in an increase in the band gap of the solid.

CONCLUSION

Our results demonstrate how the remarkable properties of clusters evolve into the properties of cluster-assembled materials in unexpected ways. Our findings, that the HOMO of the alkali metal countercation and the degree of charge transfer play important roles in determining the band gaps of these cluster-assembled solids, open the possibility of tuning the electronic properties of other cluster assemblies through systematic choices of the alkali/Crypt cations and their combinations. Developing new polyvalent anions with varying valence configurations through covalent bonding of the existing clusters with other elements offers an additional method for controlling the band gaps of cluster assemblies. Thus, linking Zintl ions through both covalent bonds, as well as electrostatic interactions, enables greater control over band gaps than possible in typical Zintl phases simply consisting of Zintl ions and alkali metals. We anticipate that this novel strategy for the development of tunable band gap materials using combinations of clusters and counterions may find applications in optoelectronics and enable the assembly of more complex materials with multiple band gaps.

MATERIALS AND METHODS

Synthesis of Cluster Assemblies (Compounds 1−7). All manipulations were performed in an argon-filled glovebox. The precursors, As_7A_3 (A = K, Rb, and Cs), were directly synthesized in scintillation vials from the corresponding elements in ethylenediamine and used for further synthetic and crystallization manipulations. The solutions were then mixed in separate scintillation vials with the appropriate reactants to prepare cluster assemblies (compounds **1**−**7**). Afterward, the suspension was filtered through a syringe filter, the solution was layered with toluene or tetrahydrofuran, and after 4−10 days crystals were recovered from the test tube. Details of the synthesis of individual assemblies are given in the Supporting Information.

Crystal Structure Determination. A suitable crystal for each compound was carefully selected under a polarizing microscope and glued to a loop. The single crystal diffraction data were collected on a Bruker APEX diffractometer with a CCD area detector at 120 K. The X-ray generator was operated at 50 kV and 32 mA using Mo Kα (λ = 0.71073 Å) radiation. Data were collected with ω scan width of 0.3°. A total of 600, 430, 235, and 50 frames were collected in three different settings of φ (0°, 90°, 180°, 270°), keeping the sample-to-detector distance fixed at 6.03 cm and the detector position (2θ) fixed at −25°. Pertinent experimental details of the structure determinations of **1**−**7** are presented in Tables S1a and S1b.

The data were reduced using SAINTPLUS,[40] and an empirical absorption correction was applied using the SADABS[41] program. The crystal structure was solved by direct methods using SHELXS97 and refined using SHELXL97 present in the SHELXTL V6.14[42] package. All non-hydrogen atoms were easily found from the different Fourier maps and refined anisotropically. For the final refinement, the hydrogen atoms were placed in geometrically ideal positions and refined using the riding mode. The last cycles of the refinement included atomic positions, anisotropic thermal parameters for all the non-hydrogen atoms, and isotropic thermal parameters for all the hydrogen atoms. Full-matrix-least-squares structure refinement against F^2 was carried out using the SHELXTL V6.14 package of programs.

Solid-State Band Gap Measurements. Diffuse reflectance spectra were collected at room temperature using a Perkin-Elmer Lambda 950 UV−vis-NIR spectrophotometer, equipped with a Harrick Praying Mantis diffuse reflectance accessory. A photomultiplier tube was used for detection in the 320−860.5 nm range, while a lead sulfide detector was used for the 860.5−2300 nm range. The spectra were collected from 320 to 2300 nm, with 1.0 nm resolution and integration times of 0.64 s. A dry and finely ground magnesium oxide (MgO) powder was used as a reflectance reference material. Prior to any measurements, all cluster-assembled materials were finely ground and diluted with MgO to 30% by weight.

Theoretical Calculations. Studies on the cluster solids were carried out using the Vienna *ab initio* stimulation package code[43] based on density functional theory (DFT). The projector augmented wave pseudopotentials[44] are taken to describe the electron-ion interaction. The generalized gradient approximation (GGA) is used for treating the exchange interactions and correlations.[45] Brillouin zone integrations have been done on Monkhorst-Pack[46] grid k-points, using the tetrahedral method. The kinetic energy cutoff of 350 eV is taken for the plane wave basis.

Studies of clusters were done using the ADF DFT code.[47] The GGA used was proposed by Perdew, Burke and Enzerhof,[45] with a TZVP basis set, the zeroth order regular approximation (ZORA) for relativistic effects was used,[48] and Hirshfeld charges were calculated to estimate charge transfer.[49]

Acknowledgment. We thank the U.S. Department of the Army (MURI Grant No. W911NF-06-1-0280) and the Kavli Foundation (P. S. W.) for financial support.

Supporting Information Available: Detailed synthesis of cluster-assemblies, procedure for the X-ray crystallography, band-gap measurements, and theoretical calculations. This material is available free of charge *via* the Internet at http://pubs.acs.org.

REFERENCES AND NOTES

1. Huynh, W. U.; Dittmer, J. J.; Alivisatos, A. P. Hybrid Nanorod−Polymer Solar Cells. *Science* **2002**, *295*, 2425–2427.
2. Murray, C. B.; Norris, D. J.; Bawendi, M. G. Synthesis and Characterization of Nearly Monodisperse CdE (E = S, Se, Te) Semiconductior Nanocrystallites. *J. Am. Chem. Soc.* **1993**, *115*, 8706–8715.
3. Warburton, R. J.; Schaflein, C.; Haft, D.; Bickel, F.; Lorke, A.; Karrai, K.; Garcia, J. M.; Schoenfeld, W.; Petroff, P. M. Optical Emission from a Charge-Tunable Quantum Ring. *Nature* **2000**, *405*, 926–929.
4. Armatas, G. S.; Kanatzidis, M. G. Hexagonal Mesoporous Germanium. *Science* **2006**, *313*, 817–820.
5. Guloy, A. M.; Ramlau, R.; Tang, Z.; Schnelle, W.; Baitinger, M.; Grin, Y. A Guest-Free Germanium Clathrate. *Nature* **2006**, *443*, 320–323.
6. Sun, D.; Riley, A. E.; Cadby, A. J.; Richman, E. K.; Korlann, S. D.; Tolbert, S. H. Hexagonal Nanoporous Germinum Through Surfactant-Driven Self-Assembly of Zintl Clusters. *Nature* **2006**, *441*, 1126–1130.
7. Korlann, S. D.; Riley, A. E.; Mun, B. S.; Tolbert, S. H. Chemical Tuning of the Electronic Properties of Nanostructured Semiconductor Films Formed through Surfactant Templating of Zintl Cluster. *J. Phys. Chem. C* **2009**, *113*, 7697–7705.
8. Riley, A. E.; Korlann, S. D.; Richman, E. K.; Tolbert, S. H. Synthesis of Semiconducting Thin Films with Nanometer-Scale Periodicity by Solution-Phase Coassembly of Zintl Clusters with Surfactants. *Angew. Chem., Int. Ed.* **2006**, *45*, 235–241.
9. Trikalitis, P. N.; Bakas, T.; Kanatzidis, M. G. Periodic Hexagonal Mesostructured Chalcogenides Based on Platinum and $[SnSe_4]^{4-}$ and $[SnSe_4]^{4-}$ Precursors. Solvent

Dependence of Nanopore and Wall Organization. *J. Am. Chem. Soc.* **2005**, *127*, 3910–3920.
10. Armatus, G. S.; Kanatzidis, M. G. Mesoporous Compound Semiconductors from the Reaction of Metal Ions with Deltahedral $[Ge_9]^{4-}$ Clusters. *J. Am. Chem. Soc.* **2008**, *130*, 11430–11436.
11. Castleman, A. W., Jr.; Khanna, S. N. Clusters, Superatoms, and Building Blocks of New Materials. *J. Phys. Chem. C* **2009**, *113*, 2664–2675.
12. Jadzinsky, P. D.; Calero, G.; Ackerson, C. J.; Bushnell, D. A.; Kornberg, R. D. Structure of a Thiol Monolayer-Protected Gold Nanoparticle at 1.1 Å Resolution. *Science* **2007**, *318*, 430–433.
13. Walter, M.; Akola, J.; Lopez-Acevedo, O.; Jadzinsky, P. D.; Calero, G.; Ackerson, C. J.; Whetten, R. L.; Gonbeck, H.; Hakkinen, H. A Unified View of Ligand-Protected Gold Clusters as Superatom Complexes. *Proc. Natl. Acad. Sci. U.S.A.* **2008**, *105*, 9157–9162.
14. Castleman, A. W., Jr.; Khanna, S. N.; Sen, A.; Reber, A. C.; Qian, M.; Davis, K. M.; Peppernick, S. J.; Ugrinov, A.; Merritt, M. D. From Designer Clusters to Synthetic Crystalline Nanoassemblies. *Nano Lett.* **2007**, *7*, 2734–2741.
15. Ugrinov, A.; Sen, A.; Reber, A. C.; Qian, M.; Khanna, S. N. $[Te_2As_2]^{2-}$: A Planar Motif with "Conflicting" Aromaticity. *J. Am. Chem. Soc.* **2008**, *130*, 782–783.
16. Bera, T. K.; Jang, J. I.; Ketterson, J. B.; Kanatzidis, M. G. Strong Second Harmonic Generation from the Tantalum Thioarsenates $A_3Ta_2AsS_{11}$ (A = K and Rb). *J. Am. Chem. Soc.* **2009**, *131*, 75–77.
17. Breaux, G. A.; Neal, C. M.; Cao, B.; Jarrold, M. F. Melting, Premelting, and Structural Transitions in Size-Selected Aluminum Clusters with around 55 Atoms. *Phys. Rev. Lett.* **2005**, *94*, 173401–173404.
18. Sanchez, A.; Abbet, S.; Heiz, U.; Schneider, W. -D.; Häkkinen, H.; Barnett, R. N.; Landman, U. When Gold Is Not Noble: Nanoscale Gold Catalysts. *J. Phys. Chem. A* **1999**, *103*, 9573–9578.
19. Socaciu, L. D.; Hagen, J.; Bernhardt, T. M.; Woste, L.; Heiz, U.; Hakkinen, H.; Landman, U. Catalytic CO Oxidation by Free Au_2^-: Experiment and Theory. *J. Am. Chem. Soc.* **2003**, *125*, 10437–10445.
20. Wang, Y.; Yamachika, R.; Wachowiak, A.; Grobis, M.; Crommie, M. Tuning Fulleride Electronic Structure and Molecular Ordering *via* Variable Layer Index. *Nat. Mater.* **2008**, *7*, 194–197.
21. Feyel, S.; Dobler, J.; Heockendorf, R.; Beyer, M. K.; Sauer, J.; Schwarz, H. Activation of Methane by Oligomeric $(Al_2O_3)_x^+$ (x = 3, 4, 5): The Role of Oxygen-Centered Radicals in Thermal Hydrogen-Atom Abstraction. *Angew. Chem., Int. Ed.* **2008**, *47*, 1946–1950.
22. Casper, J. S.; Hagenmuller, P.; Pouchard, M.; Cros, C. Clathrate Structure of Silicon Na_8Si_{46} and Na_xSi_{136} ($x < 11$). *Science* **1965**, *150*, 1713–1714.
23. Mudring, A.-V.; Corbett, J. D. Importance of Cations in the Properties of Zintl Phases: The Electronic Structure of and Bonding in Metallic Na_6TlSb_4. *Inorg. Chem.* **2005**, *44*, 5636–5640.
24. Mudring, A. V.; Corbett, J. D. Unusual Electronic and Bonding Properties of the Zintl Phase Ca_5Ge_3 and Related Compounds. A Theoretical Analysis. *J. Am. Chem. Soc.* **2004**, *126*, 5277–5281.
25. Claridge, S. A.; Castleman, A. W., Jr.; Khanna, S. N.; Murray, C. B.; Sen, A.; Weiss, P. S. Cluster-Assembled Materials. *ACS Nano* **2009**, *3*, 244–255.
26. Zintl, E. Intermetallische Verbindungen. *Angew. Chem.* **1939**, *52*, 1–6.
27. *Chemistry, Structure, and Bonding of Zintl Phases and Ions*; Kauzlarich, S. M., Ed.; VCH: New York, 1996.
28. Emmerling, F.; Röhr, C. Alkaline Metal Arsenides A_3As_7 and AAs (A = K, Rb, Cs). Preparation, Crystal Structure, Vibrational Spectroscopy. *Z. Naturforsch., B:* **2002**, *57*, 963–975.
29. von Schnering, H. G.; Somer, M.; Kiche, G.; Honle, W.; Meyer, T.; Wolf, J.; Ohse, L.; Kempa, P. B. Darstellung, Eigenschaften und Schwingungsspektren der Käfiganionen P_{11}^{3-} und As_{11}^{3-}. *Z. Anorg. Allg. Chem.* **1991**, *601*, 13–30.
30. Please see Supporting Information.
31. Kubelka, P. New Contributions to the Optics of Intensely Light Scattering Materials. I. *J. Opt. Soc. Am.* **1948**, *38*, 448–457.
32. Kubelka, P. New Contributions to the Optics of Intensely Light Scattering Materials. II. Non-homogeneous Layers. *J. Opt. Soc. Am.* **1954**, *44*, 330–335.
33. Murphy, A. B. Modified Kubelka–Munk Model for Calculation of the Reflectance of Coatings With Optically-Rough Surfaces. *J. Phys. D: Appl. Phys.* **2006**, *39*, 3571–3581.
34. Tauc, J.; Grigorocici, R.; Vacnu, A. Optical Properties and Electronic Structure of Amorphous Germanium. *Phys. Status Solidi* **1966**, *15*, 627–637.
35. Tauc, J. *The Optical Properties of Solids*; Abeles, F., Ed.; North-Holland: Amsterdam, The Netherlands, 1972.
36. Johnson, E. J. *Optical Properties of III–V Compounds, Semiconductors and Semimetals.*; Willardson, R. K., Beers, A. C., Eds.; Academic Press: New York, 1967; Vol. 3.
37. Laidani, N.; Bartali, R.; Gottardi, G.; Anderle, M. Optical Absorption Parameters of Amorphous Carbon Films from Forouhi–Bloomer and Tauc–Lorentz Models: A Comparative Study. *J. Phys.: Condens. Matter* **2008**, *20*, 015216.
38. Haddon, R. C. Electronic Structure, Conductivity and Superconductivity of Alkali Metal Doped C_{60}. *Acc. Chem. Res.* **1992**, *25*, 127–133.
39. Cohen, A. J.; Mori-Sánchez, P.; Yang, W. Insights into Current Limitations of Density Functional Theory. *Science* **2008**, *321*, 792–794.
40. *SMART*, version 5.628; *SAINT*, version 6.45a; *XPREP*; *SHELXTL*; Bruker AXS Inc.: Madison, WI, 2004.
41. Sheldrick, G. M. *Siemens Area Correction Absorption Correction Program*; University of Göttingen: Göttingen, Germany, 1994.
42. Sheldrick, G. M. *SHELXL-97 Program for Crystal Structure Solution and Refinement*; University of Göttingen: Göttingen, Germany, 1997.
43. Kresse, G.; Furthmuller, J. Efficient Iterative Schemes for *ab Initio* Total-Energy Calculations Using a Plane-Wave Basis Set. *Phys. Rev. B* **1996**, *54*, 11169–11186.
44. Kresse, G.; J. Joubert, J. From Ultrasoft Pseudopotentials to the Projector Augmented-Wave Method. *Phys. Rev. B* **1999**, *59*, 1758–1775.
45. Perdew, J. P.; Burke, K.; Enzerhof, M. Generalized Gradient Approximation Made Simple. *Phys. Rev. Lett.* **1996**, *77*, 3865–3868.
46. Monkhorst, H. J.; Pack, J. D. Special Points for Brillouin-Zone Integrations. *Phys. Rev. B* **1976**, *13*, 5188–5192.
47. G. te Velde, F. M. B.; Baerends, E. J.; Fonseca Guerra, C.; van Gisbergen, S. J. A.; Snijders, J. G.; Ziegler, T. Chemistry with ADF. *J. Comput. Chem.* **2001**, *23*, 931–967.
48. van Lenthe, E.; Baerends, E. J.; Snijders, J. G. Relativistic Regular Two-Component Hamiltonians. *J. Chem. Phys.* **1993**, *99*, 4597–4610.
49. Hirschfeld, F. L. Bonded-Atom Fragments for Describing Molecular Charge Densities. *Theor. Chim. Acta* **1977**, *44*, 129–138.